# Pseudorotational Epitaxy of Self-Assembled Octadecyltrichlorosilane Monolayers on Sapphire (0001)

H.-G. Steinrück,[1] A. Magerl,[1] M. Deutsch,[2] and B. M. Ocko[3,*]
[1]Crystallography and Structural Physics, University of Erlangen-Nürnberg, 91058 Erlangen, Germany
[2]Physics Department and Institute of Nanotechnology, Bar-Ilan University, Ramat-Gan 52900, Israel
[3]Condensed Matter Physics and Materials Science Department, Brookhaven National Lab, Upton, New York 11973, USA
(Received 17 April 2014; revised manuscript received 7 August 2014; published 6 October 2014)

The structure of octadecyltrichlorosilane self-assembled monolayers (SAMs) on sapphire (0001) was studied by Å-resolution surface-specific x-ray scattering methods. The monolayer was found to consist of three sublayers where the outermost layer corresponds to vertically oriented, closely packed alkyl tails. Laterally, the monolayer is hexagonally packed and exhibits pseudorotational epitaxy to the sapphire, manifested by a broad scattering peak at zero relative azimuthal rotation, with long powderlike tails. The lattice mismatch of ~1%–3% to the sapphire's and the different length scale introduced by the lateral Si-O-Si bonding prohibit positional epitaxy. However, the substrate induces an intriguing increase in the crystalline coherence length of the SAM's powderlike crystallites when rotationally aligned with the sapphire's lattice. The increase correlates well with the rotational dependence of the separation of corresponding substrate-monolayer lattice sites.

DOI: 10.1103/PhysRevLett.113.156101 PACS numbers: 68.35.bm, 64.75.Yz, 68.35.Ct, 68.43.Hn

Self-assembled monolayers (SAMs) have been intensely studied since their inception in the 1980s [1–4]. Their many applications range from organic field-effect transistors [5], photovoltaic devices [6], biosensors [7], and enzyme electrodes [8] to adhesion promoters [9] and lubricants [10]. For basic science, they are intriguing model systems for the study of self-organization in two-dimensional matter under the complex interplay of van der Waals (VDW), covalent, and electrostatic interactions [2]. They also provide deep insights into the principles underlying the formation, structure, and possible control of interfaces separating different-symmetry-ordered as well as different-scale-ordered bulks and thin films, a broad subject loosely termed epitaxy. Epitaxy affects a wide range of research and application areas, ranging from strained surface layer relaxation [11] through quasicrystal film formation [12], quantum structures [13], and microelectromechanical systems [14] to biomimetic thin-film growth processes [15], biomineralization [16], and the stacking of lipid bilayers [17]. Thus, the novel pseudorotational epitaxy uncovered here has potentially wide-ranging implications in many fields.

The most widely studied SAMs are alkylsilanes on the native oxide of silicon [1]. However, being amorphous, the native oxide cannot promote epitaxy; the observed hexagonal order of the SAM originates from the chain-chain VDW interaction. In addition, the different chain-chain spacing and Si-O-Si bond length [18] frustrate the lateral packing and yield a reduced crystalline coherence length, $\xi$, as discussed below.

Here we explore how a highly ordered substrate, single-crystal sapphire $Al_2O_3$ (0001), affects the structure of an octadecyltrichlorosilane (OTS) SAM. This choice of substrate was motivated by its match, both in hexagonal symmetry and in near spacing of the lattice, with the OTS alkyl chains. The sapphire's in-plane lattice constant, $a_{sap} = 4.76$ Å [19], is only 1.2% smaller than that of the OTS monolayer on silicon. This small mismatch was expected to increase the probability of commensurate epitaxy as occurs in the initial growth of Ge on Si [20], where the 4.8% lattice mismatch is fourfold larger. Surprisingly, this expectation did not materialize here, as shown below. Instead, a novel type of epitaxy, pseudorotational epitaxy, emerged.

Sample preparation followed standard procedures [2–4,21,22] detailed in the Supplemental Material [23]. Surface-specific x-ray scattering measurements yielded a detailed submolecular-resolution determination of the SAM's structure, hitherto studied on sapphire only by low-resolution, or macroscopic, methods like AFM, XPS, and ellipsometry [24]. The ultrasmooth sapphire enables high-resolution x-ray reflectivity measurements of the SAM's vertical structure, revealing a monolayer of standing-up molecules. Laterally, the SAM consists of vertically aligned molecules, with closely packed, fully extended alkyl chains exhibiting hexagonal order, as does the underlying sapphire, but with a lattice mismatch of 1% at room temperature. The two lattices exhibit a novel type of epitaxial relation where the sapphire imparts to the SAM's crystallites a preferred azimuthal orientation with a large angular width and powderlike tails in the scattering profiles. This is in contrast to existing experimental evidence and theory for substrate-monolayer epitaxy, where identical symmetry, but different lattice constant, usually yields a compression and relative azimuthal

 

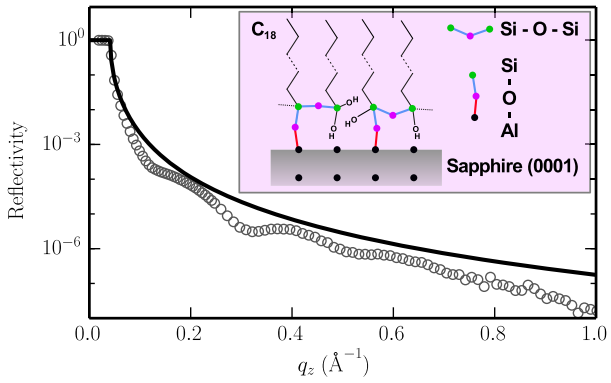


FIG. 1 (color online). Measured (symbols) x-ray reflectivity curve $R(q_z)$ for an OTS SAM on sapphire and the corresponding Fresnel $R_F(q_z)$ curve (line) of an ideally flat and abrupt sapphire surface. Inset: schematic representation of the OTS SAM monolayer on a sapphire substrate. Chemical bonds are shown as solid lines.

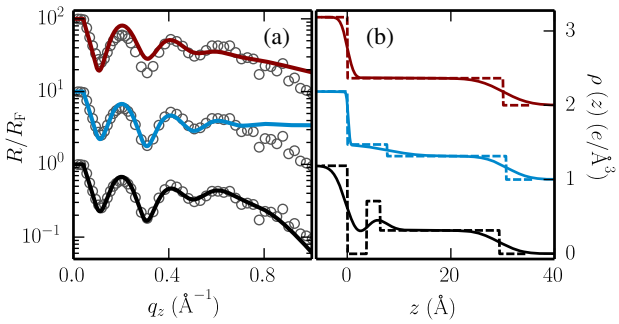


FIG. 2 (color online). (a) Fresnel-normalized measured XRR (symbols) of OTS on sapphire and the corresponding model fits (lines) for one- (brown), two- (blue) and three-slab (black) models, vertically spaced for clarity. (b) The same-color fit-derived electron density profiles with (solid lines) and without (dotted lines) surface roughness.

rotation of the substrate and monolayer lattices [25–35]. In addition, $\xi$ is found to increase as the relative azimuthal rotation angle, $\varphi$, decreases to zero. This increase is shown to correlate well with the angular dependence of the separation of corresponding sites in the monolayer and substrate lattices. We now discuss these results in detail.

The SAM's vertical structure, shown schematically in the inset of Fig. 1, was determined by x-ray reflectivity (XRR) [36] using the setup described previously [5]. XRR measures $R(q_z)$, the reflected intensity fraction of an x-ray beam of wavelength $\lambda$ incident on the SAM at a grazing angle $\alpha$. $q_z = (4\pi/\lambda)\sin\alpha$ is the surface-normal scattering vector. The measured XRR is shown in Fig. 1 along with the Fresnel XRR of an ideally smooth and abrupt interface, $R_F(q_z)$. Note the large measurable range, up to $q_z \sim 1$ Å$^{-1}$, yielding high spatial resolution. This is due to the very low roughness of the sapphire, $\sigma_0 \approx 2$ Å. The Kiessig-like fringes [36] observed in Fig. 1 are due to interference of rays reflected from the SAM's top and bottom interfaces, and yield an estimate of the SAM's thickness, $d = 2\pi/(\Delta q_z) \approx 33$ Å, based on the fringes' periodicity, $\Delta q_z \approx 0.19$ Å$^{-1}$. This $d$ is significantly larger than the 24–26 Å calculated for the molecular length [37,38], and the 23–27 Å refined from XRR measurements for the same SAM on native $SiO_2$ which forms on the silicon surface [38–40]. To elucidate the origin of this large discrepancy, and the SAM's internal structure, a detailed modeling of the surface-normal structure is required.

Following previous studies [19,41], the SAM's surface-normal electron density, $\rho(z)$, is modeled by a stack of one, two, or three "slabs," each of uniform, but variable, electron density, $\rho_i$, and thickness, $d_i$. A Gaussian roughness of width $\sigma_i$ is assumed at each interface. An additional slab with $d_0 = \infty$, $\rho_0 = 1.18\ e/$Å$^3$, and roughness $\sigma_0$ represents the sapphire. This model $\rho_m(z)$ is then used to calculate analytically the corresponding model XRR, which is least-squares fitted to the measured XRR curves [42–44]. The fit yields the best values for the model-defining parameters: $\rho_i$, $d_i$, and $\sigma_i$.

Figure 2(a) shows the best fits in solid lines, and the corresponding $\rho(z)$ profiles, in the same colors, in Fig. 2(b). A one-slab model, which accounted well for octadecanol monolayers on sapphire [19], clearly provides here a poor fit. A two-slab model, used successfully for OTS SAMs on native $SiO_2$ [39,45], provides a better fit. However, the resultant SAM thickness, 30.7 Å, is significantly larger than the extended molecule's length, 26–27 Å, and the fit-refined substrate roughness, 0.3 Å, is too small to be physical. Similar unphysical roughness values also appear for OTS on silicon; together, they suggest a limitation of the previous model [39,45]. In order to solve this conundrum we have constructed a three-slab model which results in physically realistic parameters and yields a near-perfect fit with $R^2$ values [46] for $R/R_F$ of 0.87, as compared to 0.33 and 0.28 for the two-slab and one-slab models, respectively. Here the top slab (3) represents the alkyl chains, the middle slab (2) represents the high-density cross-linking region of lateral Si-O-Si bonds [18], and the bottom slab (1) represents the substrate-adjacent low-density region of the headgroup-substrate bonds (Fig. 1, inset). As the fit is only weakly sensitive to the values of $\rho_1$ and $\rho_2$, they were fixed, respectively, to zero and the density of silicon, $\rho \approx 0.7\ e/$Å$^3$. $d_3$ and $\rho_3$ were also fixed at values calculated for close-packed, vertically aligned, extended alkyl chains, 23 Å and 0.32 $e/$Å$^3$, respectively. Furthermore, the roughnesses of the sapphire and of slab 1 were fixed at 2 Å. $d_1$, $d_2$, $\sigma_2$, and $\sigma_3$ were then fitted, yielding, respectively, $d_1 = 3.7 \pm 0.1$ Å, $d_2 = 2.7 \pm 0.1$ Å, $\sigma_2 = 2.1 \pm 0.2$ Å, and $\sigma_3 = 3.5 \pm 0.1$ Å. See the Supplemental Material [23], which includes Refs. [43,47], for parameter confidence analysis and discussion of the correlation between fitted parameters. The total SAM thickness, 29.4 Å, is now closer to the 27 Å measured thickness of OTS on native $SiO_2$ [39] and the extended molecular length derived from

the 1.27 Å molecular-axis-projected C–C distance [48]. The discrepancy of a few Å may in part reflect both incomplete silane-sapphire bonding of the silane group with the sapphire and the lattice corrugation from the incommensurate lattice.

The SAM's lateral order was explored by grazing-incidence diffraction (GID). Here the incidence angle of the x rays, $\alpha$, is kept small and the detector scanned out of the reflection plane by an angle $2\theta$, yielding a lateral diffraction vector $q_r \approx (4\pi/\lambda)\sin\theta$, which probes the surface-parallel order [36]. Using a vertically aligned linear detector, the $q_z$ distribution of the scattered intensity at each $q_r$, known as the Bragg rod (BR), was measured simultaneously. The SAM's epitaxy was explored by GID scans at different azimuthal substrate rotations, $\varphi$, relative to the sapphire's $(10\bar{1}0)$ peak.

Figure 3(a) shows the BR of the single GID peak found at $T = 25$ °C. This peak indicates a lateral hexagonal molecular order within the SAM. The absence of higher-order peaks is typical of rotator phases [41,49,50]. The BR's $q_z \approx 0$ Å$^{-1}$ peak in Fig. 3(a) indicates vertically aligned molecules [41]. As the peaks' $q_r$ position is $\varphi$ independent (see below), this attests to the powderlike nature of the OTS monolayer. In Fig. 3(b), the broad azimuthal distribution from the SAM (red circles) is in contrast to the sharp, resolution-limited peak from the uncoated substrate (black circles). The SAM is predominately rotationally aligned with the sapphire because both azimuthal ($\varphi$) scans peak at the same position. The sapphire peak in Fig. 3(b) is weak since the $\varphi$ scan was measured at the position of the SAM's $q_r$ peak position, which is somewhat smaller than the sapphire's.

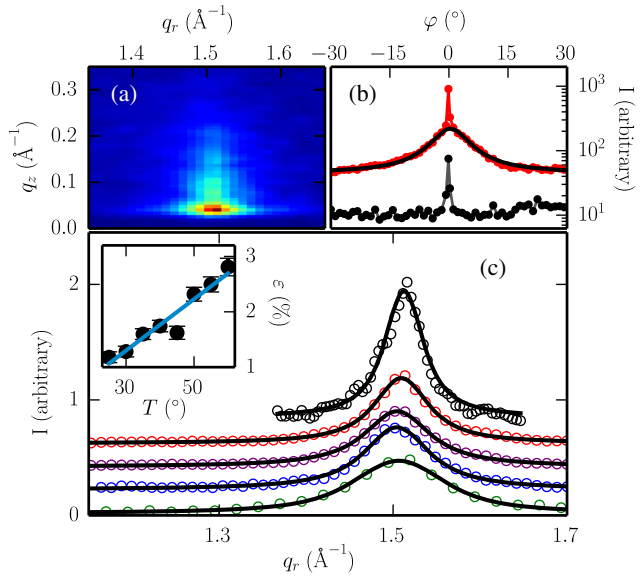


FIG. 3 (color online). (a) Grazing incidence x-ray diffraction intensity map in the $(q_r, q_z)$ plane showing a Bragg rod, originating in the OTS monolayer. (b) Measured intensity variation (red line) upon azimuthal substrate rotation, $\varphi$, at $q_r = 1.505 \pm 0.010$ Å$^{-1}$ and its Lorentzian fit (thick black line). A bare substrate scan is also shown (black line). (c) Measured (symbols) GID peaks at different azimuthal rotations, and their Lorentzian fits (lines), for $\varphi = 0.1°$ (black), 1° (red), 2° (purple), 3° (blue), and 20° (green). Inset: SAM-sapphire lattice constant mismatch $\varepsilon$ vs temperature $T$.

The SAM's azimuthal scattering peak in Fig. 3(b) is well fitted (black solid line) by a Lorentzian profile of a full width at half maximum of $(10.0 \pm 0.2)°$ (excluding the very sharp sapphire peak at $\varphi = 0$) and a constant intensity at large $\varphi$. The constant term is suggestive of powderlike behavior; further support is provided by the position of the $\varphi$-independence of the positions of the $q_r$ peaks (see below).

The $q_r$ peak widths in Fig. 3(c) exhibit $\varphi$-dependent behavior. Thus, the measured curves were fitted by a Lorentzian [39], $I(q_r) = (I_0\kappa_r/2\pi)/[(q_r - q_0)^2 + (\kappa_r/2)^2]$, convoluted with the measured Gaussian resolution function, where $\kappa_r$ is the intrinsic radial scattering width. The fits (lines) demonstrate the $\varphi$ independence of the peak position at $q_0 = 1.505 \pm 0.010$ Å$^{-1}$. The corresponding lattice constant, $a_{\mathrm{OTS}} = 4\pi/(\sqrt{3}q_0) = 4.82$ Å, is ~1% larger than the sapphire's $a_{\mathrm{sap}} = 4.76$ Å [19], which prohibits a perfect epitaxy between the monolayer and the substrate. The 4.82 Å lattice constant is very close to its value for OTS on the native $SiO_2$ surface [50] and for surface frozen alkane monolayers [51], suggesting that the spacing originates from the chain-chain VDW interactions. In contrast, the Si-O-Si lateral bond length is 3.3 Å [52], shorter than $a_{\mathrm{OTS}}$; on the native $SiO_2$ surface it has been suggested that this difference is the origin of the short $\xi$ [18], discussed next.

The $\varphi$-dependent widths, $\kappa_r$, yield $\xi$ of the SAM's 2D crystallites through the Debye-Scherrer formula, $\xi \approx (0.9 \times 2\pi)/\kappa_r$ [53,54]. $\xi(\varphi)$, shown in Fig. 4, varies from $(120 \pm 6)$ Å at $\varphi = 0.1°$ to $(60 \pm 5)$ Å at $\varphi = 20°$. The last value agrees well with the $\xi \approx 65$ Å for OTS on native $SiO_2$, calculated from previous measurements [50]. That $\xi$ is, however, $\varphi$ independent due to the amorphous nature of the underlying oxide.

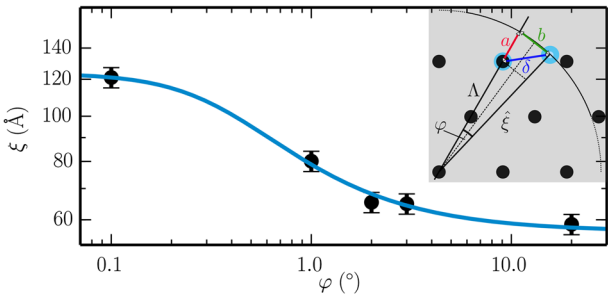


FIG. 4 (color online). Crystalline coherence length, $\xi$, of the OTS's crystallites as a function of the substrate's azimuthal rotation $\varphi$ from the in-plane sapphire peak. The line is the fit to the model discussed in the text. Inset: Sketch illustrating the displacement $\delta$ as discussed in the text.

To determine the SAM's thermal evolution, GID measurements were repeated for temperatures up to 60 °C at $\varphi = 20°$. While $\kappa_r$, and hence $\xi$, are found to be $T$ independent, the lattice mismatch, $\varepsilon = (a_{\mathrm{OTS}} - a_{\mathrm{sap}})/a_{\mathrm{sap}}$, shown in the inset to Fig. 3(c), increases linearly from 1.2% at 25 °C to 2.8% at 60 °C, yielding an areal expansion coefficient $\alpha_A = (dA/dT)/A = 0.94 \times 10^{-3}$ K$^{-1}$ where $A$ is the molecular area of the OTS. Interestingly, the same $\alpha_A$ is obtained for OTS on native $SiO_2$ [55] despite the absence of preferred orientational order. The absence of cross-linking in purely VDW-bound organic monolayers of alkanes, alcohols, and fatty acids, supported either on their own melt or on liquid mercury [51,55], results in an $\alpha_A$ that is 40%–100% larger than that found here.

Next we discuss the substrate-monolayer epitaxy, an important and extensively studied subject [28,56]. Several theoretical approaches have been developed to account for epitaxy in these systems [31–35]. However, no single theoretical model has emerged as yet for describing the rich epitaxial behavior experimentally observed for overlayers, and some important systems, e.g., halogens and alkalis on metals, are still not understood [25,34]. In hexagonal systems, e.g., atomic monolayers on graphite [30] and on single-crystal metal facets [25,26], and graphene on metals [27–29], the monolayer-substrate lattice mismatch relaxes by a combination of compression and relative azimuthal rotation of the substrate and overlayer lattices. The rotation angle depends on the corrugation potential landscape of the substrate, the substrate-monolayer interaction strength, and the elastic properties of the monolayer. These factors induce in many systems rotation angles in the substrate's symmetry, or nonsymmetry, azimuthal directions [25,31,32]. Moreover, the rotation angles are few and sharply defined. In contrast, Figs. 3 and 4 demonstrate that here a broad central peak is observed in the $\varphi$ scans with 2D powderlike tails. This, along with the $\varphi$ independence of $a_{\mathrm{OTS}}$, demonstrates that a crystallite rotation is not accompanied here by an elastic lattice relaxation. The monolayer's lattice does not lock into that of the underlying substrate even though the lattice mismatch is small, only 1.2%. Thus, the epitaxy is very weak. Nevertheless, it is still sufficiently strong to induce an increase in $\xi$ for crystallites closely aligned with the substrate's lattice, i.e., $\varphi \approx 0$. Furthermore, the weakness of the epitaxy suggests that a relatively small fraction of chains binds covalently to the surface; i.e., a large fraction of headgroups are cross-linked but not surface bound, and the epitaxial behavior is, hence, largely VDW in nature. A large fraction of covalently surface-bound molecules would imply a much stronger epitaxial behavior and would likely prohibit the broad azimuthal orientation distribution of crystallites found here. Since XRR shows a high coverage, similar to OTS on silicon [38–40], it can be concluded that these two systems are very similar in terms of lateral headgroup cross-linking.

The $\varphi$ dependence of $\xi$, shown in Fig. 4, can be rationalized as follows. For large $\varphi$ an intrinsic $\varphi$-independent $\xi_0 \approx 60$ Å is observed, identical with that observed for OTS on native amorphous $SiO_2$ [50]. $\xi_0$ is likely determined by the VDW interaction of the OTS alkyl tails and the lateral Si-O-Si bonds of the OTS headgroups. In addition, Fig. 4 shows that $\xi$ must include a term which increases with decreasing $\varphi$, presumably as a result of the increasing rotational epitaxy to the substrate. This term can be obtained by a simple geometrical argument as follows. Assume two identical overlapping hexagonal lattices, a crystal and an overlayer, with an interface-normal rotation axis through a coinciding lattice site. Expand now the overlayer lattice by a multiplicative factor of $(1 + \varepsilon)$, displacing an overlayer site a distance $\Lambda$ from the axis by $a = \Lambda\epsilon$ relative to the crystal site. An azimuthal rotation by an angle $\varphi$ displaces the overlayer site further by a distance $b = 2\Lambda(1 + \varepsilon)\sin(\varphi/2)$. Simple geometry (Fig. 4 inset) shows that this will cause the overlayer site to move away from its initially coinciding substrate site by a distance $\delta = \sqrt{a^2 + b^2 - 2ab\cos(90° - \varphi/2)} = \Lambda\sqrt{\varepsilon^2 + 4(1 + \varepsilon)\sin^2(\varphi/2)}$. Once $\delta$ exceeds some critical value $\eta$ (which may be a fraction of, or the full, nearest-neighbor distance in the bottom lattice), the two lattice sites may be considered to cease being epitaxially related to each other. However, all overlayer sites at distances shorter than $\hat{\xi}$ from the rotation axis will have $\delta < \eta$ and, hence, remain epitaxial to the substrate. Thus, $\eta$ imposes a $\varphi$-dependent limit, $\eta/\sqrt{\varepsilon^2 + 4(1 + \varepsilon)\sin^2(\varphi/2)}$, on the radius $\hat{\xi}$ inside which the two lattices may be considered epitaxially related. Making now the reasonable assumption that epitaxy causes the increase in the overlayer's crystalline coherence length $\xi$ over $\xi_0$, we can write $\xi = \xi_0 + \hat{\xi} = \xi_0 + \eta/\sqrt{\varepsilon^2 + 4(1 + \varepsilon)\sin^2(\varphi/2)}$. For a more realistic, nonabrupt loss of epitaxy with increasing $\hat{\xi}$, contributions to this loss from crystal defects, possible very small $\varepsilon$ variation upon rotation, etc., $\xi$ can be generalized to $\xi = \xi_0 + \eta/\sqrt{\varepsilon^2 + 4B(1 + \varepsilon)\sin^2(\varphi/2)}$, where $B$ is a fit parameter. In spite of its simplicity this *ad hoc* expression seems to capture the main features of the $\varphi$ variation of $\xi$, as demonstrated by its good fit to the (admittedly few) measured $\xi$ values, shown in Fig. 4, which yields $\xi_0 = 57$ Å, $\eta = 0.87$ Å, and $B = 4.5$. This said, it is clear that a more physical, molecular-level model that accounts for the disorder-inducing Si-O-Si bonds is required to fully account for $\xi(\varphi)$ and the unusual type of epitaxy found here, which we denote as pseudorotational epitaxy. Such a theory should take into consideration all lateral molecular interactions within the overlayer, and those between the overlayer and the substrate's corrugation potential.

This Letter provides an unprecedentedly detailed, Å-resolution, description of the surface-normal and surface-parallel structure of an OTS monolayer self-assembled on an ordered sapphire substrate. XRR shows the monolayer

to be ~2.5 Å thicker than the extended molecular length. This may reflect both an incomplete silane-sapphire bonding and the lattice corrugation from the incommensurate lattice. GID measurements demonstrate that the OTS monolayer consists of surface-normal-aligned molecules, ordered hexagonally, as does the underlying sapphire (0001) facet. However, the monolayer's lattice constant, larger by ~1%, prevents perfect epitaxy between the two lattices. In previously studied similar systems, the mismatch relaxes by an azimuthal rotation of the two lattices by a single (or few) sharply defined angle [31,34,35], or, for a small, few-percent, mismatch, remain unrotated, in spite of the energy cost of the resultant strain [25,33]. Here, the monolayer exhibits a very broad distribution of the crystallite's azimuthal rotation with powderlike tails and a rotation-independent lattice constant, implying a weak epitaxial relation, which enhances the crystallites' azimuthal orientation and crystalline coherence length $\xi$, as $\varphi = 0$ is approached. The latter correlates quantitatively with the separation of corresponding lattice sites in the substrate and the monolayer. This constitutes an intermediate type of epitaxy, denoted here as pseudorotational epitaxy, where no positional or rotational epitaxy exists between substrate and monolayer, yet the monolayer's crystalline properties ($\xi$ and crystallite orientation in this case) are influenced by epitaxy to the substrate. To our knowledge, such behavior has not been hitherto reported, and we hope that this Letter will lead to theoretical treatments of such systems.

Financial support through the DFG research unit 1878, "Functional Molecular Structures on Complex Oxide Surfaces," is gratefully acknowledged. We thank Alexei Tkachenko (BNL) for important discussions and the U.S.-Israel Binational Science Foundation, Jerusalem, for support. Work at BNL is supported by the Division of Materials Sciences (DOE) under Contract No. DE-AC02-76CH0016.

*ocko@bnl.gov

[1] C. D. Bain, E. B. Troughton, Y. T. Tao, J. Evall, G. M. Whitesides, and R. G. Nuzzo, J. Am. Chem. Soc. **111**, 321 (1989); J. Sagiv, *ibid.* **102**, 92 (1980).
[2] S. Onclin, B. J. Ravoo, and D. N. Reinhoudt, Angew. Chem. **44**, 6282 (2005).
[3] F. Schreiber, Prog. Surf. Sci. **65**, 151 (2000); D. K. Schwartz, Annu. Rev. Phys. Chem. **52**, 107 (2001).
[4] A. Ulman, Chem. Rev. **96**, 1533 (1996).
[5] M. Halik and A. Hirsch, Adv. Mater. **23**, 2689 (2011); S. G. J. Mathijssen *et al.*, Nat. Nanotechnol. **4**, 674 (2009); T. Schmaltz, A. Y. Amin, A. Khassanov, T. Meyer-Friedrichsen, H.-G. Steinrück, A. Magerl, J. J. Segura, K. Voitchovsky, F. Stellacci, and M. Halik, Adv. Mater. **25**, 4511 (2013); E. C. P. Smits *et al.*, Nature (London) **455**, 956 (2008).
[6] R. J. Kline, M. D. Mcgehee, and M. F. Toney, Nat. Mater. **5**, 222 (2006).
[7] J. N. Anker, W. P. Hall, O. Lyandres, N. C. Shah, J. Zhao, and R. P. Van Duyne, Nat. Mater. **7**, 442 (2008); N. K. Chaki and K. Vijayamohanan, Biosens. Bioelectron. **17**, 1 (2002).
[8] J. J. Gooding and D. B. Hibbert, Trends Anal. Chem. **18**, 525 (1999).
[9] D. G. Kurth and T. Bein, Langmuir **11**, 3061 (1995).
[10] X. D. Xiao, J. Hu, D. H. Charych, and M. Salmeron, Langmuir **12**, 235 (1996).
[11] J. Tersoff and F. K. LeGoues, Phys. Rev. Lett. **72**, 3570 (1994).
[12] S. Foerster, K. Meinel, R. Hammer, M. Trautmann, and W. Widdra, Nature (London) **502**, 215 (2013).
[13] J. Wu and Z. M. Wang, J. Phys. D **47**, 173001 (2014); C. V. Falub, H. von Kaenel, F. Isa, R. Bergamaschini, A. Marzegalli, D. Chrastina, G. Isella, E. Mueller, P. Niedermann, and L. Miglio, Science **335**, 1330 (2012).
[14] S. H. Baek *et al.*, Science **334**, 958 (2011).
[15] I. Aksay, M. Trau, S. Manne, I. Honma, N. Yao, L. Zhou, P. Fenter, P. M. Eisenberger, and S. M. Gruner, Science **273**, 892 (1996).
[16] S. Mann, D. D. Archibald, J. M. Didymus, T. Douglas, B. R. Heywood, F. C. Meldrum, and N. J. Reeves, Science **261**, 1286 (1993).
[17] L. Tayebi, Y. Ma, D. Vashaee, G. Chen, S. K. Sinha, and A. N. Parikh, Nat. Mater. **11**, 1074 (2012).
[18] R. Maoz, S. Matlis, E. DiMasi, B. Ocko, and J. Sagiv, Nature (London) **384**, 150 (1996); R. Maoz, J. Sagiv, D. Degenhardt, H. Möhwald, and P. Quint, Supramol. Sci. **2**, 9 (1995).
[19] B. M. Ocko, H. Hlaing, P. N. Jepsen, S. Kewalramani, A. Tkachenko, D. Pontoni, H. Reichert, and M. Deutsch, Phys. Rev. Lett. **106**, 137801 (2011).
[20] H. Ye and J. Yu, Sci. Tech. Adv. Mater. **15**, 024601 (2014).
[21] K. Wen, R. Maoz, H. Cohen, J. Sagiv, A. Gibaud, A. Desert, and B. M. Ocko, ACS Nano **2**, 579 (2008).
[22] S. P. Pujari, L. Scheres, A. T. M. Marcelis, and H. Zuilhof, Angew. Chem., Int. Ed. Engl. **53**, 6322 (2014).
[23] See Supplemental Material at http://link.aps.org/supplemental/10.1103/PhysRevLett.113.156101 for sample preparation procedures and fit parameter confidence analysis.
[24] L. N. Mitchon and J. M. White, Langmuir **22**, 6549 (2006).
[25] G. S. Leatherman and R. D. Diehl, Phys. Rev. B **53**, 4939 (1996).
[26] O. Magnussen, Chem. Rev. **102**, 679 (2002); O. M. Magnussen, B. M. Ocko, R. R. Adzic, and J. X. Wang, Phys. Rev. B **51**, 5510 (1995); B. M. Ocko, G. M. Watson, and J. Wang, J. Chem. Phys. **98**, 897 (1994).
[27] J. Coraux, A. T. N'Diaye, C. Busse, and T. Michely, Nano Lett. **8**, 565 (2008).
[28] J. Wintterlin and M.-L. Bocquet, Surf. Sci. **603**, 1841 (2009).
[29] D. Franz, S. Runte, C. Busse, S. Schumacher, T. Gerber, T. Michely, M. Mantilla, V. Kilic, J. Zegenhagen, and A. Stierle, Phys. Rev. Lett. **110**, 065503 (2013).
[30] K. L. D'Amico, D. E. Moncton, E. D. Specht, R. J. Birgeneau, S. E. Nagler, and P. M. Horn, Phys. Rev. Lett. **53**, 2250 (1984).

[31] J. P. McTague and A. D. Novaco, Phys. Rev. B **19**, 5299 (1979).
[32] F. Grey and J. Bohr, Europhys. Lett. **18**, 717 (1992).
[33] H. Shiba, J. Phys. Soc. Jpn. **46**, 1852 (1979); **48**, 211 (1980).
[34] A. C. Hillier and M. D. Ward, Phys. Rev. B **54**, 14037 (1996).
[35] A. Tkatchenko, Phys. Rev. B **74**, 035428 (2006).
[36] P. S. Pershan and M. L. Schlossman, *Liquid Surfaces and Interfaces: Synchrotron X-Ray Methods* (Cambridge University Press, Cambridge, England, 2012); M. Deutsch and B. M. Ocko, *Encyclopedia of Applied Physics*, edited by G. L. Trigg (VCH, New York, 1998), Vol. 23; M. Tolan, *X-ray Scattering from Soft Matter Thin Films* (Springer, Berlin, 1999); J. Als-Nielsen and D. McMorrow, *Elements of Modern X-ray Physics* (Wiley, New York, 2001).
[37] T. Koga, K. Honda, S. Sasaki, O. Sakata, and A. Takahara, Langmuir **23**, 8861 (2007).
[38] T. Ishizaki, N. Saito, S. H. Lee, and O. Takai, Nanotechnology **19**, 055601 (2008).
[39] I. M. Tidswell, B. M. Ocko, P. S. Pershan, S. R. Wasserman, G. M. Whitesides, and J. D. Axe, Phys. Rev. B **41**, 1111 (1990); M. Mezger, S. Schöder, H. Reichert, H. Schröder, J. Okasinski, V. Honkimäki, J. Ralston, J. Bilgram, R. Roth, and H. Dosch, J. Chem. Phys. **128**, 244705 (2008).
[40] K. Kojio, A. Takahara, K. Omote, and T. Kajiyama, Langmuir **16**, 3932 (2000).
[41] B. M. Ocko, X. Z. Wu, E. B. Sirota, S. K. Sinha, O. Gang, and M. Deutsch, Phys. Rev. E **55**, 3164 (1997); L. Tamam, B. M. Ocko, H. Reichert, and M. Deutsch, Phys. Rev. Lett. **106**, 197801 (2011).
[42] F. Abeles, J. Phys. Radium **11**, 307 (1950).
[43] A. Nelson, J. Appl. Crystallogr. **39**, 273 (2006).
[44] Analysis was carried out using the Abeles transfer matrix method as implemented in MOTOFIT.
[45] A. G. Richter, M. K. Durbin, C. J. Yu, and P. Dutta, Langmuir **14**, 5980 (1998).
[46] A. C. Cameron and F. A. G. Windmeijer, J. Econometrics **77**, 329 (1997).
[47] F. Heinrich, T. Ng, D. J. Vanderah, P. Shekhar, M. Mihailescu, H. Nanda, and M. Lsche, Langmuir **25**, 4219 (2009).
[48] D. M. Small, *The Physical Chemistry of Lipids* (Plenum, New York, 1986).
[49] V. M. Kaganer, H. Mohwald, and P. Dutta, Rev. Mod. Phys. **71**, 779 (1999); I. Kuzmenko, V. M. Kaganer, and L. Leiserowitz, Langmuir **14**, 3882 (1998).
[50] I. M. Tidswell, T. A. Rabedeau, P. S. Pershan, S. D. Kosowsky, J. P. Folkers, and G. M. Whitesides, J. Chem. Phys. **95**, 2854 (1991).
[51] B. M. Ocko, E. Sirota, M. Deutsch, E. DiMasi, S. Coburn, J. Strzalka, S. Zheng, A. Tronin, T. Gog, and C. Venkataraman, Phys. Rev. E **63**, 032602 (2001).
[52] R. C. Weast, *CRC Handbook of Chemistry and Physics*, 54th ed. (CRCPress, New York, 1974).
[53] L. Tamam, H. Kraack, E. Sloutskin, B. M. Ocko, and M. Deutsch, Phys. Rev. B **85** (2012).
[54] A. Guinier, *X-Ray Diffraction* (Freeman, San Francisco, 1963).
[55] H. G. Steinrück, M. Deutsch, B. M. Ocko, and A. Magerl (to be published); E. Sloutskin, H. Kraack, B. Ocko, J. Ellmann, M. Moller, P. Lo Nostro, and M. Deutsch, Langmuir **18**, 1963 (2002); H. Kraack, B. M. Ocko, P. S. Pershan, E. Sloutskin, L. Tamam, and M. Deutsch, Langmuir **20**, 5375 (2004); **20**, 5386 (2004).
[56] G. A. Somorjai, *Introduction to Surface Chemistry and Catalysis* (Wiley, New York, 1994); Y. H. Wu, T. Yu, and Z. X. Shen, J. Appl. Phys. **108**, 071301 (2010).